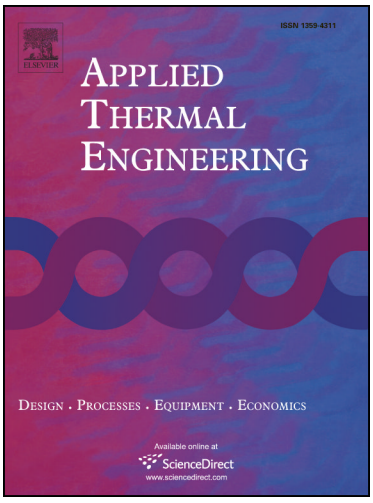

Research Paper

Appropriate utilization of the unit cell method in thermal calculation of composites

Jian-Jun Gou, Chun-Lin Gong, Wen-Quan Tao

PII: S1359-4311(17)37002-3
DOI: https://doi.org/10.1016/j.applthermaleng.2018.04.127
Reference: ATE 12124

To appear in: *Applied Thermal Engineering*

Received Date: 2 November 2017
Revised Date: 8 April 2018
Accepted Date: 26 April 2018

Please cite this article as: J-J. Gou, C-L. Gong, W-Q. Tao, Appropriate utilization of the unit cell method in thermal calculation of composites, *Applied Thermal Engineering* (2018), doi: https://doi.org/10.1016/j.applthermaleng.2018.04.127

Appropriate utilization of the unit cell method in thermal calculation of composites

Jian-Jun Gou[1]*, Chun-Lin Gong[1], Wen-Quan Tao[2]

[1] Shaanxi Aerospace Flight Vehicle Key Laboratory, School of Astronautics, Northwestern Polytechnical University, Xi'an 710072, China

[2] Key Laboratory of Thermo-Fluid Science and Engineering, Ministry of Education, School of Energy & Power Engineering, Xi'an Jiaotong University, Xi'an 710049, China

* Correspondent authors: jj.gou@nwpu.edu.cn

Abstract

The unit cell method is widely used in thermal calculations of composite. The formulation of a unit cell involves the construction of geometric configuration and the derivation of boundary conditions. The process is closely related to the structure symmetries of composites and the macro heat flux. In this work, two issues are studied to further appropriate utilization of such method. First, unit cells that formulated based on different paths of different structure symmetries could have the same configuration while different boundary conditions, and leads to some confusions; second, the uniform temperature boundary condition is frequently used without rigorous mathematical derivation and physical consideration, and leaves some uncertainty of its reliability. In this work, three typical composites, unidirectional fiber reinforced, plain woven and three-dimensional four-directional braided composites are studied. For each composite, one unit cell is formulated and two types of boundary conditions are derived. The influence of formulation path on unit cell formulation and the application scope of uniform temperature boundary conditions are then clarified based on corresponding calculations and analysis.

Keywords*: thermal conduction*; *composite*; *unit cell*; *boundary condition*

Nomenclature

Abbreviation

ATS	antisymmetric thermal stimulus

BC	boundary condition
BCa, BCb	boundary condition derived from Path a and b, respectively
RVE	representative volume element
STS	symmetric thermal stimulus
UBC	uniform temperature boundary condition
UC, UC1, UC2, UC3	unit cell and numbered ones
UD	unidirectional fiber reinforced
1D, 2D, 3D	one-, two-, three-dimensional
3D4d	three-dimensional four-directional
symbols	
a	length of unit cell in x-direction
b	length of unit cell in y-direction
h	length of unit cell in z-direction
q_i, q_i^0	local and macro heat flux in i direction
T	temperature
x, y, z	coordinate direction
λ_i^0	effective thermal conductivity in i direction
$\nabla T_i^0, \nabla T_x^0, \nabla T_y^0, \nabla T_z^0$	macro temperature gradients in i-, x-, y-, z-direction
subscripts	
x_1, y_1, z_1	coordinates of node

1. Introduction

For a high-speed vehicle like hypersonic one, the surface temperature may reach a value of 1600℃ or even higher [1, 2] in a very short time of hundreds of seconds. Under this condition, a reliable and efficient thermal protection system (TPS) is required, and the thermal characteristics of relevant TPS composites should be deeply studied.

The effective thermal properties of composites can be efficiently calculated by a representative volume element (RVE) model. According to the structure of composites, there are two types of RVE can be formulated. For composites with random phase distributions such as needled composites (randomly distributed short fibers) [3, 4], fiber layers in proton exchange membrane fuel cell (randomly distributed short fibers and pores) [5-8], porous materials (random pores) [9-11], granular composite (random

reinforcing granula) [12] and thermal barrier coatings (random pores) [13, 14], the RVE is formulated based on statistical parameters (e.g., phase volume fraction) of the composite structure. Due to the structure stochasticity, such RVE is an approximate rather than accurate model.

For another type of composite with certain geometric symmetries such as textile reinforced composites [15-26] and idealized foam materials [27-30], the RVE can be formulated based on structure symmetries. Such RVE is the so-called unit cell (UC). In composites, any complex symmetric structures can be decomposed into three types of symmetric structures: translation along an axis, reflection about a plane and rotation about an axis for a certain angle (mainly 180°) [31]. The translational symmetry is always used to formulate a full UC first, and the other two symmetries can then be used to reduce the unit cell size. Each UC needs corresponding boundary condition (BC) to represent the macro structure. The derivation of BC should be based on rigorous mathematical and thermo-physical considerations [32]. In most above Refs. [15-19, 22, 23], only translational symmetries are employed to formulate unit cells, and the periodic relative temperature or periodic temperature gradient are the appropriate BC for such unit cells. In the authors' works about plain woven [20], satin woven [32, 33], three-dimensional four-directional braided (3D4d) [34] composites, the reflectional and 180° rotational symmetries are used to formulate unit cells, and the results show that such two symmetries will reduce the UC size while lead to more complicated BC.

Compare with the RVE of randomly structured composites, a UC model of symmetrically structured composites can be theoretically accurate in representing the macro composite; however, the formulation of an accurate UC is relatively complicated. In general, it involves construction of geometric configuration and derivation of BC, and the process is closely related to the structure symmetries and macro thermal condition (heat flux/temperature gradient field) of the composite. At present, the complex coupling relation between these four factors needs further studies, mainly in two aspects. First, in previous literatures, the utilization of different combination of symmetries (expressed as UC formulation path in this work) means different

configurations and different BC of the UC; however, sometimes different symmetries may formulate the same geometric configuration and meanwhile the derived BC are still different; this brings about some confusions in simulations and needs to be clarified. Second, the typical uniform temperature BC (UBC) is very easy to apply, good for convergence, and thus preferred by many simulations; however, sometimes it is used without rigorous mathematical derivations or physical considerations [24, 35, 36], this leaves some uncertainty; thus the application scope of UBC should be determined.

In this work, three typical composites, the unidirectional (UD) fiber reinforced, plain woven and 3D4d braided composites are studied. Such three composites can represent fiber yarns, 2D woven, 3D braided composites, respectively. For each composite, one UC is formulated by two different paths. Then based on corresponding calculations and analysis, the influence of formulation path on UC formulation is clarified and the application scope of UBC is determined.

2. Constitutive equations

For a thermal conduction problem, e.g., the calculation of effective thermal conductivities of composites, the constitutive relation between macro heat flux and temperature gradient is shown in Eq. (1).

$$q_i^0 = -\boldsymbol{\lambda}^0 \nabla T_i^0, i = x, y, z \tag{1}$$

where q_i^0 is the macro (global) heat flux, $\boldsymbol{\lambda}^0$ is the effective thermal conductivity, ∇T_i^0 is the macro temperature gradient, and *i* is the component direction. For a specific case, if one of q_i^0 and ∇T_i^0 is given as boundary conditions, the other one will be obtained by solving heat differential equation and appropriate post-processing, and the effective thermal conductivities $\boldsymbol{\lambda}^0$ can then be calculated based on Eq. (1).

3. Two formulation paths of the unit cell

As discussed above, the unit cell is established based on three types of structure symmetries, i.e., translation along an axis, reflection about a plane and 180° rotation about an axis. For a specific composite, a UC can be formulated based on a certain path. Sometimes different formulation paths will build up the same

UC configuration. In order to study the influence of formulation path, typical paths should be discussed first for UD, plain woven and 3D4d braided composites. It should be noted that these three types of composites are studied because: first, UD composite is relevant to all textile reinforced composites since the textile fiber yarn is a sort of UD composite; second, the plain woven composite is a typical 2D woven composite with laminar structures, while 3D4d braided composite is the representative of 3D braided composite; third, the formulation paths (see later subsections) of UC for these composites involves all structure symmetries and their combinations. It should be mentioned again that three types of structure symmetries, i.e., translational, reflectional and 180° rotational symmetries are used to formulate UC in this work.

Figures 1, 2 and 3 show different paths from composite to unit cells for UD, plain woven and 3D4d braided composite, respectively. It has to be stated that all the three composites are anisotropic while transverse-isotropic, and thus the UC formulation can be discussed in transverse direction and axial direction, respectively.

3.1 UD composite

Figure 1(a) is the unit cell formulation in transverse (*x*-, *y*-) direction, while the lower Fig. 1(b) is the axial (*z*-) direction. UC1 of black lines, UC2 with blue background, and UC3 with white background are three unit cells of reducing size. The right part of Fig. 1(a) lists three paths from composite to each unit cell. It should be noted that UC3 is the smallest UC that can be formulated by translational symmetries, and it will be used to conduct the simulation in this work. UC3 can be formulated based on three paths, Path a: translational symmetries along *x*- and *y*-direction by periodic lengths of (*a*, *b*); Path b: translational symmetries along *x*- and *y*-direction by periodic lengths of (2*a*, 2*b*), and additional reflectional symmetries about P_x^1 and P_y^1 (indicated in structure of UC2); Path c: translational symmetries along *x*- and *y*-direction by periodic lengths of (4*a*, 4*b*), additional reflectional symmetries about P_x^0 and P_y^0 (indicated in structure of UC1), and further reflectional symmetries about P_x^1 and P_y^1 (indicated in structure of UC2).

In the axial direction as shown in Fig.1 (b), the structure has translational symmetries of arbitrary periodic lengths, which means that the UC can have an arbitrary height. UC1, UC2 and UC3 can be formulated by translational symmetries directly, and at the same time, there are corresponding reflectional symmetries between them. The three formulation paths are very similar to that listed in Fig. 1(a). To be summarized for UD composites, UC3 has three paths (Path a, b and c).

3.2 Plain woven composite

Figure 2 shows the formulation paths from plain woven composites to multi-size unit cells. Plain woven composite has typical laminated structure. Figure 2(a) is the transverse (*x*-, *y*-) direction while Fig. 2(b) is the axial direction. As shown in Fig. 2(b), the mainly difference with that of UD composite is in the axial direction: UC1, UC2 and UC3 can only be formulated by one path, i.e., translational symmetries by certain periodic length, and the length must be multiples of a single laminate (height of UC3). To be summarized for plain woven composites, UC3 has three paths (Path a, b and c), and no reflectional symmetries exist in axial direction.

3.3 Three-dimensional four-directional braided composite

Figure 3 shows the formulation paths from 3D4d braided composites to multi-size unit cells. Compared with the plain woven composite, the structure of 3D4d braided composite is more complex and has totally different formulation paths. As shown in the upper right part of Fig. 3, the mainly difference is in the transverse direction, between UC1, UC2 and UC3, there are 180° rotational symmetries rather than reflectional ones. For the axial (*z*-) direction, 3D4d braided composite has the same situation with plain woven composite. To be summarized for 3D4d braided composites, UC3 has three paths (Path a, b, c), and no reflectional symmetries exist in all directions.

In fact, for the axial (*z*-) direction of 3D4d composite, one can also formulate UC1 based on some 180° rotational symmetries indicated in UC2 structure, and UC2 can also be formulated based on that of UC1. In

this work such paths are not considered for the case of paper length, and only the translational symmetry is considered in *z*-direction.

3.4 Path summary and unit cell models

The formulation paths from composites to UC3 are summarized in Table 1. The dimension of all the UC3 is assumed to be $a \times b \times h$. In later discussions, it is used to conduct the example calculation for each composite. UC3 can be formulated by three paths: Path a, the one based on translational symmetries only; Path b and c, the combination of translational and other two types of symmetries. In this work, both Path a and Path b are considered to derive two types of boundary conditions, BCa and BCb. It leads to a confusion that one UC can have two different boundary conditions. Therefore, in later sections, BCa is used to conduct corresponding calculations, and the numerical results on boundaries are compared with BCb and the confusion is thus clarified.

Figure 4 shows the UC3 models for UD, plain woven and 3D4d braided composites, respectively. The red region is the fibers or fiber yarns while the blue region is the matrix. The right lower diagram is the schematic of formulation Path a, which is based on three translational symmetries along *x*-, *y*-, and *z*-axis. All the UC models can be simplified as a cube with dimension of $a \times b \times h$, which specifically are $1 \times 1.732 \times 0.25$ mm, $1.92 \times 1.92 \times 0.34$ mm and $2.49 \times 2.49 \times 4.318$ mm for UD, plain woven and 3D4d braided composites, respectively. For plain woven composite, the cross section and the axis of fiber yarns are defined by cosine functions and similar configurations can be found in [20]. For a 3D4d unit cell, according to the discussion in [21], its geometric configuration is closely related to two parameters, i.e., the interior braiding angle (the angle between fiber yarns and *z*-axis), and the fiber volume fraction which are 30° and 0.5 in this work, respectively. Also, the elliptical cross-sectional fiber yarns are adopted in the model establishment.

4. Boundary conditions from different paths

4.1 Macro thermal stimuli

For reflectional and 180° rotational symmetric structures, the direction of macro heat flux will influence the derivation of BC. In this work if the macro heat flux is parallel to the reflection plane or the 180° rotation axis, it will be defined as symmetric thermal stimulus (STS), while if perpendicular it will be antisymmetric one (ATS). Under STS and ATS, for reflectional and 180° rotational symmetric structures, the relative temperature relations between symmetric nodes (*M* and *M'*) are summarized as two equations, Eq. (2) and Eq. (3), respectively:

$$\text{STS:}\quad T_M - T_O = T_{M'} - T_{O'} \tag{2}$$

$$\text{ATS:}\quad T_M - T_O = T_{O'} - T_{M'} \tag{3}$$

where *O* is the reference node and *O'* is its symmetric node. The two equations are confirmed by corresponding calculations, and the physical meanings are stated in [32]. When *M* comes to a boundary, the STS and ATS equations can be used to derived BC of unit cells. It should be noted that for translational symmetric structures, all the macro heat flux will have STS expression, and Eq. (2) can be used to derived relevant BC.

In this work, the boundary planes of UC3 are expressed as P_1 ~ P_6 as shown in Fig. 5. The structure symmetries used in the formulation of each boundary plane (Path b) are summarized in Table 2. The BC of each plane are derived based on the periodic BC of UC2 and the relevant symmetries listed in Table 2. As discussed above, for reflectional and 180° rotational symmetries, the macro heat flux (q_x^0, q_y^0 and q_z^0) should be considered as STS or ATS by its relative relations to symmetric planes or axes. In Table 2, for each boundary plane, q_x^0, q_y^0 and q_z^0 are listed as STS or ATS, and it is very important for the BC derivation of corresponding planes. Take P_1 of UD composites as an instance, during the Path b of UC3, P_1 is relevant to a translational symmetry along *x*-axis and a further reflectional symmetry about plane P_x^0 which is perpendicular to *x*-axis. Under this condition, the macro heat fluxes q_x^0, q_y^0 and q_z^0 which are perpendicular,

parallel and parallel to P_x^0, respectively, can be considered as ATS, STS and STS, respectively. It should be noted that for translational symmetric structures, no matter the macro heat flux is perpendicular or parallel to the translational axis, the relative temperature relations between symmetric nodes satisfy periodic distribution.

For UC3, the boundary conditions derived base on Path a and b can be expressed as BCa and BCb, respectively. BCa is derived by translational symmetries, and should be the periodic BC, while BCb is that derived based on the periodic one for UC2 with additional reflectional or 180° rotational symmetries. BCa has a well-known expression, thus the key point of next subsection is to derive BCb for each composite.

4.2 Boundary conditions from Path a

For three types of composites, the periodic BCa has the expression as shown in Eq. (4). The relative temperature relations of corresponding nodes are in periodic distributions. The ∇T_x^0, ∇T_y^0 and ∇T_z^0 in equations are the macro temperature gradients in *x*-, *y*- and *z*-direction, respectively. Equation (4-1) is the BC of nodes on boundary planes excluding those on edges and vertices, this is because during the applying of such BC, the nodes on edges and vertices are always over constrained: the nodes on a specific edge will be constrained by BC equations of the two adjacent planes, and the nodes on a specific vertex will be constrained by BC equations of the three adjacent edges. In commercial software like ANSYS or ABAQUS, such redundant constraints will stop the program running. Therefore, the BC of edges and vertices should be derived and imposed on separately. Equations (4-2) and (4-3) are the boundary conditions of edges and vertices, respectively, and they can be derived based on Eq. (4-1). The edges and vertices are indicated by numbers with black and white circles, respectively, as shown in Fig. 5. Equation (4) will be used to conduct relevant simulations.

Planes :

$$\begin{aligned}
&\boldsymbol{P_1}-\boldsymbol{P_2}: T_{(0,y_1,z_1)}-T_{(a,y_1,z_1)}=a\nabla T_x^{\,0}\\
&\boldsymbol{P_3}-\boldsymbol{P_4}: T_{(x_1,0,z_1)}-T_{(x_1,b,z_1)}=b\nabla T_y^{\,0}\\
&\boldsymbol{P_5}-\boldsymbol{P_6}: T_{(x_1,y_1,0)}-T_{(x_1,y_1,h)}=h\nabla T_z^{\,0}
\end{aligned} \tag{4-1}$$

Edges :

$$\begin{aligned}
&9-17: T_{(0,0,z_1)}-T_{(a,0,z_1)}=a\nabla T_x^{\,0}\\
&9-11: T_{(0,0,z_1)}-T_{(0,b,z_1)}=b\nabla T_y^{\,0}\\
&9-14: T_{(0,0,z_1)}-T_{(a,b,z_1)}=a\nabla T_x^{\,0}+b\nabla T_y^{\,0}\\
&10-16: T_{(0,y_1,0)}-T_{(a,y_1,0)}=a\nabla T_x^{\,0}\\
&10-12: T_{(0,y_1,0)}-T_{(0,y_1,h)}=h\nabla T_z^{\,0}\\
&10-18: T_{(0,y_1,0)}-T_{(a,y_1,h)}=a\nabla T_x^{\,0}+h\nabla T_z^{\,0}\\
&19-13: T_{(x_1,0,0)}-T_{(x_1,b,0)}=b\nabla T_y^{\,0}\\
&19-20: T_{(x_1,0,0)}-T_{(x_1,0,h)}=h\nabla T_z^{\,0}\\
&19-15: T_{(x_1,0,0)}-T_{(x_1,b,h)}=b\nabla T_y^{\,0}+h\nabla T_z^{\,0}
\end{aligned} \tag{4-2}$$

Vertices :

$$\begin{aligned}
&1-2: T_{(0,0,0)}-T_{(a,0,0)}=a\nabla T_x^{\,0}\\
&1-3: T_{(0,0,0)}-T_{(a,b,0)}=a\nabla T_x^{\,0}+b\nabla T_y^{\,0}\\
&1-4: T_{(0,0,0)}-T_{(0,b,0)}=b\nabla T_y^{\,0}\\
&1-5: T_{(0,0,0)}-T_{(0,0,h)}=h\nabla T_z^{\,0}\\
&1-6: T_{(0,0,0)}-T_{(a,0,h)}=a\nabla T_x^{\,0}+h\nabla T_z^{\,0}\\
&1-7: T_{(0,0,0)}-T_{(a,b,h)}=a\nabla T_x^{\,0}+b\nabla T_y^{\,0}+h\nabla T_z^{\,0}\\
&1-8: T_{(0,0,0)}-T_{(0,b,h)}=b\nabla T_y^{\,0}+h\nabla T_z^{\,0}
\end{aligned} \tag{4-3}$$

4.3 Boundary conditions from Path b

The second formulation Path b will lead to totally different boundary conditions, BCb. Before the derivation of BCb, the periodic BC for UC2 should be stated first as shown in Eq. (5). BCb can then be derived based on Eq. (5) and relevant structure symmetries indicated in UC2.

The derivation processes for UD, plain woven and 3D four-directional braided composites are listed in Tables 3, 4 and 5, respectively. The derived BCb of UD, plain woven and 3D4d braided composites are shown in Eqs. (6), (7) and (8), respectively. It should be noted that the BC described in Eqs. (5) ~ (8) will not be directly used in calculations, thus the constraint equations on edges and vertices are not displayed. In all

the equations, the subscript represents the coordinate of node. x_1, y_1 and z_1 mean the coordinates of nodes on a specific plane or edge; a, b and h are lengths of unit cell in x-, y- and z- direction, respectively.

$$\begin{aligned}
&\boldsymbol{P_1}-\boldsymbol{P_2}: T_{(0,y_1,z_1)}-T_{(2a,\,y_1,z_1)}=2a\nabla T_x^{\,0}\\
&\boldsymbol{P_3}-\boldsymbol{P_4}: T_{(x_1,0,z_1)}-T_{(x_1,\,2b,z_1)}=2b\nabla T_y^{\,0}\\
&\boldsymbol{P_5}-\boldsymbol{P_6}: T_{(x_1,y_1,0)}-T_{(x_1,y_1,2h)}=2h\nabla T_z^{\,0}
\end{aligned} \tag{5}$$

Boundary conditions for UD composites:

Under $q^0{}_x$:
$$\begin{aligned}
&\boldsymbol{P_1}: T_{(0,y_1,z_1)}-T_{(0,0,0)}=0\\
&\boldsymbol{P_2}: T_{(a,y_1,z_1)}-T_{(0,0,0)}=-a\nabla T_x^{\,0}
\end{aligned} \tag{6-1}$$

Under $q^0{}_y$:
$$\begin{aligned}
&\boldsymbol{P_3}: T_{(x_1,0,z_1)}-T_{(0,0,0)}=0\\
&\boldsymbol{P_4}: T_{(x_1,b,z_1)}-T_{(0,0,0)}=-b\nabla T_y^{\,0}
\end{aligned} \tag{6-2}$$

Under $q^0{}_z$:
$$\begin{aligned}
&\boldsymbol{P_5}: T_{(x_1,y_1,0)}-T_{(0,0,0)}=0\\
&\boldsymbol{P_6}: T_{(x_1,y_1,h)}-T_{(0,0,0)}=-h\nabla T_z^{\,0}
\end{aligned} \tag{6-3}$$

For plain woven composites:

Under $q^0{}_x$:
$$\begin{aligned}
&\boldsymbol{P_1}: T_{(0,y_1,z_1)}-T_{(0,0,0)}=0\\
&\boldsymbol{P_2}: T_{(a,y_1,z_1)}-T_{(0,0,0)}=-a\nabla T_x^{\,0}\\
&\boldsymbol{P_5}-\boldsymbol{P_6}: T_{(x_1,y_1,0)}-T_{(x_1,y_1,h)}=0
\end{aligned} \tag{7-1}$$

Under $q^0{}_y$:
$$\begin{aligned}
&\boldsymbol{P_3}: T_{(x_1,0,z_1)}-T_{(0,0,0)}=0\\
&\boldsymbol{P_4}: T_{(x_1,b,z_1)}-T_{(0,0,0)}=-b\nabla T_y^{\,0}\\
&\boldsymbol{P_5}-\boldsymbol{P_6}: T_{(x_1,y_1,0)}-T_{(x_1,y_1,h)}=0
\end{aligned} \tag{7-2}$$

Under $q^0{}_z$:
$$\boldsymbol{P_5}-\boldsymbol{P_6}: T_{(x_1,y_1,0)}-T_{(x_1,y_1,h)}=h\nabla T_z^{\,0} \tag{7-3}$$

For 3D four-directional braided composites:

Under $q^0{}_x$:
$$\begin{aligned}
&\boldsymbol{P_1}: T_{(0,y_1,z_1)}+T_{(0,y_1,h-z_1)}-2T_{(0,0,0)}=0\\
&\boldsymbol{P_2}: T_{(a,y_1,z_1)}+T_{(a,y_1,h-z_1)}-2T_{(0,0,0)}=-2a\nabla T_x^{\,0}\\
&\boldsymbol{P_3}: T_{(x_1,0,z_1)}-T_{(x_1,0,h-z_1)}=0\\
&\boldsymbol{P_4}: T_{(x_1,b,z_1)}-T_{(x_1,b,h-z_1)}=0\\
&\boldsymbol{P_5}-\boldsymbol{P_6}: T_{(x_1,y_1,0)}-T_{(x_1,y_1,h)}=0
\end{aligned} \tag{8-1}$$

$$
\begin{aligned}
&\boldsymbol{P_1}: T_{(0,y_1,z_1)} - T_{(0,y_1,h-z_1)} = 0 \\
&\boldsymbol{P_2}: T_{(a,y_1,z_1)} - T_{(a,y_1,h-z_1)} = 0 \\
\text{Under } q^0{}_y: \quad &\boldsymbol{P_3}: T_{(x_1,0,z_1)} + T_{(x_1,0,h-z_1)} - 2T_{(0,0,0)} = 0 \\
&\boldsymbol{P_4}: T_{(x_1,b,z_1)} + T_{(x_1,b,h-z_1)} - 2T_{(0,0,0)} = -2b\nabla T_y{}^0 \\
&\boldsymbol{P_5} - \boldsymbol{P_6}: T_{(x_1,y_1,0)} - T_{(x_1,y_1,h)} = 0
\end{aligned}
\tag{8-2}
$$

$$
\begin{aligned}
&\boldsymbol{P_1}: T_{(0,y_1,z_1)} + T_{(0,y_1,h-z_1)} - 2T_{(0,0,0)} = -h\nabla T_z{}^0 \\
&\boldsymbol{P_2}: T_{(a,y_1,z_1)} + T_{(a,y_1,h-z_1)} - 2T_{(0,0,0)} = -h\nabla T_z{}^0 \\
\text{Under } q^0{}_z: \quad &\boldsymbol{P_3}: T_{(x_1,0,z_1)} + T_{(x_1,0,h-z_1)} - 2T_{(0,0,0)} = -h\nabla T_z{}^0 \\
&\boldsymbol{P_4}: T_{(x_1,b,z_1)} + T_{(x_1,b,h-z_1)} - 2T_{(0,0,0)} = -h\nabla T_z{}^0 \\
&\boldsymbol{P_5} - \boldsymbol{P_6}: T_{(x_1,y_1,0)} - T_{(x_1,y_1,h)} = h\nabla T_z{}^0
\end{aligned}
\tag{8-3}
$$

It should be noted that BC in Eqs. (4) and (5) can be used to simulate heat conductions in three directions ($q_x{}^0$, $q_y{}^0$ and $q_z{}^0$) at the same time, however, that in Eqs. (6), (7) and (8) are derived in three directions separately. This is because for translational symmetries, the macro heat flux in all directions can be considered as the same stimulus (STS), and Eq. (2) can be used to derive BC under all conditions ($q_x{}^0$, $q_y{}^0$ and $q_z{}^0$), thus a unified form can be obtained; while for reflectional and 180° rotational symmetries, the different direction of macro heat flux will lead to totally different Eqs. (2) or (3), thus the BC should be derived in three conditions, separately. This indicates that under a 3D heat conduction problem, only the UC that formulated and the BC that derived by translational symmetries are available; for 2D problems, the UC that formulated by reflectional or 180° rotational symmetries are also available under certain conditions, i.e., when the heat flux components are the same stimulus.

The derivation process listed in Tables 3, 4 and 5 should be described in more details, take case $q_x{}^0$ in Table 3 as an instance: for P_1 and P_2 the macro heat flux can be considered as ATS (see Table 2), then BC of P_1 and P_2 can be derived based on Eq. (5) and Eq. (2) (ATS); for P_3 ~ P_6 the macro heat flux can be considered as STS (see Table 2), then BC of P_3 ~ P_6 can be derived based on Eq. (5) and Eq. (1) (STS); finally, the BCb of UC3 under $q_x{}^0$ can be derived as shown in Eq. (6-1). Similar processes can be found for cases of $q_y{}^0$ and $q_z{}^0$, and also for other two types of composites in Tables 4 and 5. The detailed BC derivation

(from Eqs. (5) and (2) or (3) to Eqs. (6) ~ (8)) can be described by the case P_1 with q_x^0 of UD composite (see Table 3):

UC3 is formulated based on UC2, and P_1 = (0, y, z) is formulated by reflectional transformation about P_x^1 = (a, y, z) (see Fig. 1). M is an arbitrary node on P_1, M' is the node that reflectional symmetric to M, then we can have coordinates of M = (0, y_1, z_1) and M' = (2a, y_1, z_1). Node O = (0, 0, 0) is assumed to be the reference node, and its symmetric node is O = (2a, 0, 0).

The macro heat flux can be considered as ATS (see Table 2), thus Eq. (3) can be used to derive BC. Express M, M', O, and O' by coordinates, Eq. (3) becomes:

$$T_{(0,y_1,z_1)} - T_{(0,0,0)} = T_{(2a,0,0)} - T_{(2a,y_1,z_1)} \tag{9}$$

According to the BC of UC2 (P_1 - P_2 in Eq. (5)), Eq. (9) can be further derived as:

$$T_{(0,y_1,z_1)} - T_{(0,0,0)} = 0 \tag{10}$$

It is clear that Eq. (10) has the same expression as the first equation of Eq. (7-1). The other derivations listed in Tables 3, 4 and 5 have the similar process, and will be omitted here. However, the reflection planes, rotation axes and translation axes relevant to each boundary should be stated here: for UD composite (Eq. (6)), P_1 and P_2 corresponds to reflection plane P_x^1 = (a, y, z), P_3 and P_4 correspond to reflection plane P_y^1 = (x, b, z), while P_5 and P_6 correspond to reflection plane P_z^1 = (x, y, h) (see Fig. 1); for plain woven composite (Eq. (7)), P_1 and P_2 correspond to reflection plane P_x^1 = (a, y, z), P_3 and P_4 correspond to reflection plane P_y^1 = (x, b, z), while P_5 and P_6 correspond to translation z-axis (see Fig. 2); for 3D4d composite (Eq. (8)), P_1 and P_2 correspond to rotation axis Ly^1 = (a, y, h/2), P_3 and P_4 correspond to rotation axis Lx^1 = (x, b, h/2), while P_5 and P_6 correspond to translation z-axis (see Fig. 3).

The characteristics of BCb as shown in Eqs. (6), (7) and (8) are summarized in Table 6. For UD composites, as indicated in Eq. (6-1), under q_x^0, the boundary planes in x-direction should have uniform temperature BC (UBC) while the boundary planes in y- and z-direction are adiabatic ones, and the same

situation can be found for the cases of q_y^0 and q_z^0. For plain woven composite, as indicated in Eq. (7-1), under q_x^0 and q_y^0, the boundary planes in *x*-direction should have UBC, while the boundary planes in *y*-direction are adiabatic and that in *z*-direction are periodic ones; under q_z^0, boundary planes in *z*-direction are periodic while in *x*- and *y*-direction are adiabatic BC. For 3D4d braided composites, as indicated in Eq. (8), for all the boundary planes in *x*- and *y*-direction, the upper part and the lower part should have constraint relations, while the boundary planes in *z*-direction are periodic conditions. According to Table 2 and Table 6, one can find that: 1st. reflectional symmetries will lead to uniform temperature distributions on the boundary planes; 2nd. the 180° rotational symmetries will bring about constraint relations between two corresponding halves (lower and upper, left and right, etc.) of a single boundary plane.

In this paper, the periodic BCa (Eq. (4)) are used to conduct the calculation, and the results on boundary planes will be compared with the temperature fields constrained by BCb (Eqs. (6), (7), (8)). If the numerical results satisfy the descriptions of BCb, it can be concluded that a unit cell can have different BC but will obtain the unique results. It means that for such a unit cell, the specific formulation path is not important provided that its BC is derived rigorously based on its own path.

5. Model discretization

Figure 6 is the meshed models for UD, plain woven and 3D4d braided composites. ANSYS Mechanical is used to conduct the calculation. The element is the 3D thermal solid element SOLID70 which is a hexahedron with 8 nodes. For UD, plain woven and 3D4d braided composites, the model has 21580 elements and 24607 nodes, 704747 elements and 236906 nodes, and 3030525 elements and 4049794 nodes, respectively. It also should be noted that the numerical results obtained in this work are independent of mesh size.

In order to apply the periodic BC, the corresponding boundary planes should be meshed identically. As shown in the right lower diagram of Fig. 6, for unit cells established in this work, the symmetric planes are

P_1 and P_2, P_3 and P_4, and P_5 and P_6.

6. Results and discussions

6.1 UD composites

Figures 7 (a), (b) and (c) are temperature fields obtained under macro heat flux in *x*-, *y*- and *z*-direction (q_x^0, q_y^0, q_z^0), respectively. In the calculation, the temperature of reference node (0, 0, 0) is assumed to be 0, and the macro temperature gradient is 20. The fields on boundary planes in calculation directions, e.g., planes $x = 0$ and $x = a$ for the case of q_x^0, are displayed separately. As shown in Fig.7, all the boundary planes have uniform temperature distributions as described in Eq. (6) and as summarized in Table 6. It means that the BC used in the simulation is derived by Path a (translational symmetries), while at the same time the results on boundaries satisfy the conditions that derived by Path b (the combination of translational and reflectional symmetries). Therefore, for UD composite, a unit cell can have different formulation paths and different boundary conditions, while unique numerical results.

6.2 Plain woven composites

Figures 8 (a), (b) and (c) are the temperature fields of plain woven composite under q_x^0, q_y^0, q_z^0, respectively. The temperature of the reference node (0, 0, 0) is 0, and the macro temperature gradient is 20. The fields on boundary planes in calculation directions are displayed, separately. As shown in Figs. 8 (a) and (b), the temperature on boundary planes $P_1 \sim P_4$ are uniform as summarized in Table 6. However, as shown in Fig. 8(c) the boundary planes P_5 and P_6 have non-uniform temperature fields. This phenomenon is very closely related to the formulation path of those boundary planes as summarized in Table 2, i.e., $P_1 \sim P_4$ can be formulated by the combination of translational and reflectional symmetries, while P_5 and P_6 can only be formulated by translational symmetries.

As shown in Fig. 8(c), if the temperature fields on P_5 and P_6 are investigated, one can find further reflectional symmetric and 180° rotational symmetric fields. The black dashed lines represent reflection

planes (perpendicular to paper) while the black circle indicates 180° rotation axis (perpendicular to paper). It worth noting that these boundary results imply corresponding structure symmetries in the UC structure as shown in Fig. 9. In Fig. 9, the matrix is not shown to display the fiber yarns clear, the two blue planes are reflection planes, and the black line is the rotation axis, and such structure symmetries can be used to further formulate unit cells with smaller size.

6.3 3D four-directional braided composites

Figures 10(a), (b) and (c) are the temperature fields of 3D4d braided composites under q_x^0, q_y^0, q_z^0, respectively. The fields on boundary planes in calculation directions are displayed. All the boundary planes ($P_1 \sim P_6$) of 3D4d braided composites have non-uniform temperature fields since the formulation path of these boundary planes are combinations of translational and 180° rotational symmetries, rather than reflectional ones. Compare the results on P_1 and P_2, translational symmetric (periodic) relations between corresponding locations can be found. The same situation can be found on P_3 and P_4, and P_5 and P_6.

If the boundary temperature fields are further investigated, 180° rotational symmetric fields can be found. The black point in boundary planes indicates the rotation axis (perpendicular to the paper). Temperature fields on P_1 & P_2 and P_3 & P_4 imply 180° rotational symmetries about axis X_1 and Y_1, respectively, while that on P_5 and P_6 indicate symmetries about Z_1 and further Z_2. Figure 11 shows the 180° rotational symmetries in the structure of the present UC. The radius of fiber bundles is smaller than that in Fig. 4 to display its orientation clear. The thick red lines are the fiber yarns while the blue lines are the rotation axes. In the right four diagrams of Fig. 11, one specific fiber bundle L_1 and its symmetric bundles are used to clarify the structure symmetries. It is clear shown that L_1 and L_1' are 180° symmetric to each other about X_1, L_1 and L_1'' are symmetric about Y_1, and L_1 and L_1''' are symmetric about Z_1, while L_1''' and L_1'''' are 180° symmetric about Z_2. Also, all these structure symmetries can be used to further formulate unit cells with smaller size.

From Figs. 9(c), 10(a), (b) and (c) one can notice that the nonuniformity on the non-isothermal boundary planes is relatively small: for *z*-plane of plain woven, transverse (*x*-, *y*-) planes of 3D4d, and *z*-plane of 3D4d braided composites are on the orders of about 1%, 6% and 2% of the global temperature scales, respectively. This means that even if rigorously wrong, the UBC can be a good and easy approximation for some problems. However, the error is dependent on several factors, e.g., the difference of thermal conductivities between fiber yarns and matrix. An additional case of 3D4d braided composite is calculated by increasing thermal conductivities (both transverse and axial) of fibers 10 times (no change of matrix), and the finally calculated nonuniformity on transverse planes increases to 13%. Therefore, it is essential to evaluate possible errors before the utilization of UBC.

6.4 Summary

First of all, according to the above discussions in this section we can obtain a conclusion: a UC can be formulated by different paths and can have different BC, whereas the numerical results are unique. For such a unit cell, the specific formulation path is not concerned provided that the BC is derived rigorously. Thus, one can choose a formulation path and derive corresponding BC that appropriate for his own work.

Secondly, the temperature on all the boundary planes ($P_1 \sim P_6$) of UD and the *x*- and *y*- boundary planes ($P_1 \sim P_4$) of plain woven composite have the same distribution with UBC, which means that for such boundary planes the UBC is fortunately correct. However, the results on *z*- boundary planes (P_5 and P_6) of plain woven and all boundary planes ($P_1 \sim P_6$) of 3D4d braided composites have totally different distributions with UBC, which means that for such boundary planes of such unit cells, UBC is incorrect. If Path b for $P_1 \sim P_6$ of UD composite and $P_1 \sim P_4$ of plain woven composite is re-examined, one can find reflectional symmetries (see Table 2). So, it can be concluded that UBC is correct for boundaries that can be formulated based on reflectional symmetries, while inappropriate for others. This gives researchers a

criterion of whether UBC is appropriate for their models, especially for the situation that complex boundary conditions are difficult to apply.

7 Conclusions

In this work, the utilization of unit cell method in thermal calculation of composites is studied and two issues, i.e., the confusion of one configuration with different boundary conditions and the application scope of uniform temperature boundary condition are clarified. Three types of composites, unidirectional fiber reinforced, plain woven and three-dimensional four-directional braided composites are studied. For each composite, one unit cell is formulated, and two types of boundary conditions are derived based on two different formulation paths: Path a of translational symmetries, and Path b of combinations of translational with reflectional or rotational symmetries. The numerical results show some conclusions:

1. A unit cell can be formulated by different paths and can have different boundary conditions, whereas the numerical results are unique. For such a unit cell, the specific formulation path is not concerned provided that the boundary condition is derived rigorously. Thus, one can choose a formulation path and derive corresponding boundary conditions that appropriate for his own work.

2. For unit cells and boundaries that can be formulated by reflectional symmetries, the widely used uniform temperature boundary condition (UBC) is correct, while for unit cells that can only be formulated by translational symmetries or 180° rotational ones, it is inappropriate. For UD composites, UBC is correct for thermal calculations in all directions; for plain woven composites, it is correct in *x*- and *y*-direction while inappropriate in *z*-direction; for three-dimensional four-directional braided composites, it is inappropriate for all directional thermal calculations.

3. The calculated temperature fields on boundary planes always indicate further structure symmetries that can be used to formulate unit cells with smaller size.

Acknowledgment:

This study is supported by the Fundamental Research Funds for the Central Universities (3102017OQD068).

References

[1] F Gori, S Corasaniti, W M Worek, and W J Minkowycz. Theoretical prediction of thermal conductivity for thermal protection systems. Applied Thermal Engineering, 2012. 49: 124-130.

[2] T Ji, R Zhang, B Sunden, and G Xie. Investigation on thermal performance of high temperature multilayer insulations for hypersonic vehicles under aerodynamic heating condition. Applied Thermal Engineering, 2014. 70(1): 957-965.

[3] J Xie, J Liang, G Fang, and Z Chen. Effect of needling parameters on the effective properties of 3D needled C/C-SiC composites. Composites Science and Technology, 2015. 117: 69-77.

[4] W Z Fang, J J Gou, H Zhang, Q Kang, and W Q Tao. Numerical predictions of the effective thermal conductivity for needled C/C-SiC composite materials. Numerical Heat Transfer, Part A: Applications, 2016. 70(10): 1101-1117.

[5] L Chen, H B Luan, Y L He, and W Q Tao. Pore-scale flow and mass transport in gas diffusion layer of proton exchange membrane fuel cell with interdigitated flow fields. International Journal of Thermal Sciences, 2012. 51: 132-144.

[6] X He, Y Guo, M Li, N Pan, and M Wang. Effective gas diffusion coefficient in fibrous materials by mesoscopic modeling. International Journal of Heat and Mass Transfer, 2017. 107: 736-746.

[7] M Wang, Q Kang, and N Pan. Thermal conductivity enhancement of carbon fiber composites. Applied Thermal Engineering, 2009. 29(2–3): 418-421.

[8] X Huang, Q Zhou, J Liu, Y Zhao, W Zhou, and D Deng. 3D stochastic modeling, simulation and analysis of effective thermal conductivity in fibrous media. Powder Technology, 2017. 320(Supplement C): 397-404.

[9] M Wang and N Pan. Modeling and prediction of the effective thermal conductivity of random open-cell porous foams. International Journal of Heat and Mass Transfer, 2008. 51(5–6): 1325-1331.

[10] P Ranut. On the effective thermal conductivity of aluminum metal foams: Review and improvement of the available empirical and analytical models. Applied Thermal Engineering, 2016. 101: 496-524.

[11] H Liu, X Xia, X Xie, Q Ai, and D Li. Experiment and identification of thermal conductivity and extinction coefficient of silica aerogel composite. International Journal of Thermal Sciences, 2017. 121(Supplement C): 192-203.

[12] J Su, X Liu, M Charmchi, and H Sun. Experimental and numerical study of anisotropic thermal conductivity of magnetically aligned PDMS/Ni particle composites. International Journal of Heat and Mass Transfer, 2016. 97: 645-652.

[13] Y Wang, H Liu, X Ling, and Y Weng. Effects of pore microstructure on the effective thermal conductivity of thermal barrier coatings. Applied Thermal Engineering, 2016. 102(Supplement C): 234-242.

[14] M Moayeri and A Kaflou. Effect of powder shape on effective thermal conductivity of Cu–Ni porous coatings. Journal of Materials Research and Technology, 2017.

[15] R P A Rocha and M A E Cruz. Computation of the effective conductivity of unidirectional fibrous composites with an interfacial thermal resistance. Numerical Heat Transfer, Part A: Applications, 2001. 39(2): 179-203.

[16] K Woo and N S Goo. Thermal conductivity of carbon-phenolic 8-harness satin weave composites. Composite Structures, 2004. 66(1-4): 521-526.

[17] P Del Puglia, M A Sheikh, and D R Hayhurst. Thermal transport property prediction of a CMC laminate from base materials properties and manufacturing porosities. Proceedings of the Royal Society a-Mathematical Physical and Engineering Sciences, 2005. 461(2063): 3575-3597.

[18] L L Jiang, G D Xu, S Cheng, X M Lu, and T Zeng. Predicting the thermal conductivity and temperature distribution in 3D braided composites. Composite Structures, 2014. 108: 578-583.

[19] K Dong, K Liu, Q Zhang, B Gu, and B Sun. Experimental and numerical analyses on the thermal conductive behaviors of carbon fiber/epoxy plain woven composites. International Journal of Heat and Mass Transfer, 2016. 102: 501-517.

[20] J J Gou, Y J Dai, S Li, and W Q Tao. Numerical study of effective thermal conductivities of plain woven composites by unit cells of different sizes. International Journal of Heat and Mass Transfer, 2015. 91: 829-840.

[21] J J Gou, H Zhang, Y J Dai, S Li, and W Q Tao. Numerical prediction of effective thermal conductivities of 3D four-directional braided composites. Composite Structures, 2015. 125: 499-508.

[22] Y Xu, H Ye, L Zhang, and Q Cai. Investigation on the effective thermal conductivity of carbonized high silica/phenolic ablative material. International Journal of Heat and Mass Transfer, 2017. 115(Part B): 597-603.

[23] J J Zhai, S Cheng, T Zeng, Z H Wang, and D N Fang. Extended multiscale FE approach for steady-state heat conduction analysis of 3D braided composites. Composites Science and Technology, 2017. 151(Supplement C): 317-324.

[24] X Gao, X Han, and Y Song. X-ray computed tomography based microstructure reconstruction and numerical estimation of thermal conductivity of 2.5D ceramic matrix composite. Ceramics International, 2017. 43(13): 9790-9797.

[25] J Zhai, S Cheng, T Zeng, Z Wang, and L Jiang. Thermo-mechanical behavior analysis of 3D braided composites by multiscale finite element method. Composite Structures, 2017. 176(Supplement C): 664-672.

[26] J J Gou, C L Gong, L X Gu, S Li, and W Q Tao. Unit cells of composites with symmetric structures for the study of effective thermal properties. Applied Thermal Engineering, 2017.

[27] K Boomsma, D Poulikakos, and Y Ventikos. Simulations of flow through open cell metal foams using an idealized periodic cell structure. International Journal of Heat and Fluid Flow, 2003. 24(6): 825-834.

[28] X Hu and S S Patnaik. Modeling phase change material in micro-foam under constant temperature condition. International Journal of Heat and Mass Transfer, 2014. 68(Supplement C): 677-682.

[29] X Hu, H Wan, and S S Patnaik. Numerical modeling of heat transfer in open-cell micro-foam with phase change material. International Journal of Heat and Mass Transfer, 2015. 88: 617-626.

[30] S S Sundarram and W Li. The effect of pore size and porosity on thermal management performance of phase change material infiltrated microcellular metal foams. Applied Thermal Engineering, 2014. 64(1): 147-154.

[31] S G Li and S R Reid. On the symmetry conditions for laminated fiber-reinforced composite structures. International Journal of Solids and Structures, 1992. 29(23): 2867-2880.

[32] J J Gou, C L Gong, L X Gu, S Li, and W Q Tao. Unit cells of composites with symmetric structures for the study of effective thermal properties. Applied Thermal Engineering, 2017. 126(Supplement C): 602-619.

[33] J J Gou, X J Ren, W Z Fang, S Li, and W Q Tao. Two small unit cell models for prediction of thermal properties of 8-harness satin woven pierced composites. Composites Part B: Engineering, 2018. 135(Supplement C): 218-231.

[34] J J Gou, W Z Fang, Y J Dai, S Li, and W Q Tao. Multi-size unit cells to predict effective thermal conductivities of 3D four-directional braided composites. Composite Structures, 2017. 163: 152-167.

[35] H Yu, D Heider, and S Advani. Prediction of effective through-thickness thermal conductivity of woven fabric reinforced composites with embedded particles. Composite Structures, 2015. 127: 132-140.

[36] H Yu, D Heider, and S Advani. Comparison of two finite element homogenization prediction approaches for through thickness thermal conductivity of particle embedded textile composites. Composite Structures, 2015. 133: 719-726.

Table Captions

Table 1 Formulation paths from composite to UC3

			UD	Plain woven	3D4d braided
UC3	*x*-, *y*-	Path a	Transl.	Transl.	Transl.
		Path b	Transl.+Refl.	Transl.+Refl.	Transl.+180° Rot.
		Path c	Transl.+Refl.+Refl.	Transl.+Refl.+Refl.	Transl.+180° Rot.+180° Rot.
	z-	Path a	Transl.	Transl.	Transl.
		Path b	Transl. + Refl.	/	/
		Path c	Transl. +Refl.+Refl.	/	/

Table 2 Structure symmetries for each boundary plane (formulation Path b)

		UD	Plain woven	3D4d braided
P_1	Symmetries	Transl. (x) + refl. ($\perp x$)	Transl. (x) + refl. ($\perp x$)	Transl. (x) + 180° rot. ($/\,/\,y$)
	q_x^0; q_y^0; q_z^0	ATS; STS; STS	ATS; STS; STS	ATS; STS; ATS
P_2	Symmetries	Transl. (x) + refl. ($\perp x$)	Transl. (x) + refl. ($\perp x$)	Transl. (x) + 180° rot. ($/\,/\,y$)
	q_x^0; q_y^0; q_z^0	ATS; STS; STS	ATS; STS; STS	ATS; STS; ATS
P_3	Symmetries	Transl. (y) + refl. ($\perp y$)	Transl. (y) + refl. ($\perp y$)	Transl. (y) + 180° rot. ($/\,/\,x$)
	q_x^0; q_y^0; q_z^0	STS; ATS; STS	STS; ATS; STS	STS; ATS; ATS
P_4	Symmetries	Transl. (y) + refl. ($\perp y$)	Transl. (y) + refl. ($\perp y$)	Transl. (y) + 180° rot. ($/\,/\,x$)
	q_x^0; q_y^0; q_z^0	STS; ATS; STS	STS; ATS; STS	STS; ATS; ATS
P_5	Symmetries	Transl. (z) + refl. ($\perp z$)	Transl. (z)	Transl. (z)
	q_x^0; q_y^0; q_z^0	STS; STS; ATS	STS; STS; STS	STS; STS; STS
P_6	Symmetries	Transl. (z) + refl. ($\perp z$)	Transl. (z)	Transl. (z)
	q_x^0; q_y^0; q_z^0	STS; STS; ATS	STS; STS; STS	STS; STS; STS

Table 3 Derivation of BCb of UD composite

	Boundary conditions	**Eq. No.**
under $q^0{}_x$	Eq. (5) +ATS Eq. (3) $\Rightarrow$ $\boldsymbol{P_1}: T_{(0,y_1,z_1)} - T_{(0,0,0)} = 0$ $\boldsymbol{P_2}: T_{(a,y_1,z_1)} - T_{(0,0,0)} = -a\nabla T_x{}^0$ Eq. (5) +STS Eq. (2) $\Rightarrow \boldsymbol{P_3}, \boldsymbol{P_4}, \boldsymbol{P_5}, \boldsymbol{P_6}$: adiabatic	(6-1)
under $q^0{}_y$	Eq. (5) +ATS Eq. (3) $\Rightarrow$ $\boldsymbol{P_3}: T_{(x_1,0,z_1)} - T_{(0,0,0)} = 0$ $\boldsymbol{P_4}: T_{(x_1,b,z_1)} - T_{(0,0,0)} = -b\nabla T_y{}^0$ Eq. (5) +STS Eq. (2) $\Rightarrow \boldsymbol{P_1}, \boldsymbol{P_2}, \boldsymbol{P_5}, \boldsymbol{P_6}$: adiabatic	(6-2)
under $q^0{}_z$	Eq. (5) +STS Eq. (2) $\Rightarrow \boldsymbol{P_1}, \boldsymbol{P_2}, \boldsymbol{P_3}, \boldsymbol{P_4}$: adiabatic Eq. (5) +ATS Eq. (3) $\Rightarrow$ $\boldsymbol{P_5}: T_{(x_1,y_1,0)} - T_{(0,0,0)} = 0$ $\boldsymbol{P_6}: T_{(x_1,y_1,h)} - T_{(0,0,0)} = -h\nabla T_z{}^0$	(6-3)

Table 4 Derivation of BCb of plain woven composite

	Boundary conditions	**Eq. No.**
under $q^0{}_x$	Eq. (5) +ATS Eq. (3) $\Rightarrow$ $\boldsymbol{P_1}: T_{(0,y_1,z_1)} - T_{(0,0,0)} = 0$ $\boldsymbol{P_2}: T_{(a,y_1,z_1)} - T_{(0,0,0)} = -a\nabla T_x{}^0$ Eq. (5) +STS Eq. (2) $\Rightarrow \boldsymbol{P_3}, \boldsymbol{P_4}$: adiabatic Periodicity $\Rightarrow \boldsymbol{P_5} - \boldsymbol{P_6}: T_{(x_1,y_1,0)} - T_{(x_1,y_1,h)} = 0$	(7-1)
under $q^0{}_y$	Eq. (5) +STS Eq. (2) $\Rightarrow \boldsymbol{P_1}, \boldsymbol{P_2}$: adiabatic Eq. (5) +ATS Eq. (3) $\Rightarrow$ $\boldsymbol{P_3}: T_{(x_1,0,z_1)} - T_{(0,0,0)} = 0$ $\boldsymbol{P_4}: T_{(x_1,b,z_1)} - T_{(0,0,0)} = -b\nabla T_y{}^0$ Periodicity $\Rightarrow \boldsymbol{P_5} - \boldsymbol{P_6}: T_{(x_1,y_1,0)} - T_{(x_1,y_1,h)} = 0$	(7-2)
under $q^0{}_z$	Eq. (5) +STS Eq. (2) $\Rightarrow \boldsymbol{P_1}, \boldsymbol{P_2}, \boldsymbol{P_3}, \boldsymbol{P_4}$: adiabatic Periodicity $\Rightarrow \boldsymbol{P_5} - \boldsymbol{P_6}: T_{(x_1,y_1,0)} - T_{(x_1,y_1,h)} = 0$	(7-3)

Table 5 Derivation of BCb of 3D four-directional composite

	Boundary conditions	**Eq. No.**
under $q^0{}_x$	Eq. (5) +ATS Eq. (3) $\Rightarrow$ $\boldsymbol{P_1}: T_{(0,y_1,z_1)} + T_{(0,y_1,2h-z_1)} - 2T_{(0,0,0)} = 0$ $\boldsymbol{P_2}: T_{(a,y_1,z_1)} + T_{(a,y_1,h-z_1)} - 2T_{(0,0,0)} = -2a\nabla T_x{}^0$ Eq. (5) +STS Eq. (2) $\Rightarrow$ $\boldsymbol{P_3}: T_{(x_1,0,z_1)} - T_{(x_1,0,h-z_1)} = 0$ $\boldsymbol{P_4}: T_{(x_1,b,z_1)} - T_{(x_1,b,h-z_1)} = 0$ Periodicity $\Rightarrow \boldsymbol{P_5} - \boldsymbol{P_6}: T_{(x_1,y_1,0)} - T_{(x_1,y_1,h)} = 0$	(8-1)
under $q^0{}_y$	Eq. (5) +STS Eq. (2) $\Rightarrow$ $\boldsymbol{P_1}: T_{(0,y_1,z_1)} - T_{(0,y_1,h-z_1)} = 0$ $\boldsymbol{P_2}: T_{(a,y_1,z_1)} - T_{(a,y_1,h-z_1)} = 0$ Eq. (5) +ATS Eq. (3) $\Rightarrow$ $\boldsymbol{P_3}: T_{(x_1,0,z_1)} + T_{(x_1,0,h-z_1)} - 2T_{(0,0,0)} = 0$ $\boldsymbol{P_4}: T_{(x_1,b,z_1)} + T_{(x_1,b,h-z_1)} - 2T_{(0,0,0)} = -2b\nabla T_y{}^0$ Periodicity $\Rightarrow \boldsymbol{P_5} - \boldsymbol{P_6}: T_{(x_1,y_1,0)} - T_{(x_1,y_1,h)} = 0$	(8-2)
under $q^0{}_z$	Eq. (5) +ATS Eq. (3) $\Rightarrow$ $\boldsymbol{P_1}: T_{(0,y_1,z_1)} + T_{(0,y_1,h-z_1)} - 2T_{(0,0,0)} = -h\nabla T_z{}^0$ $\boldsymbol{P_2}: T_{(a,y_1,z_1)} + T_{(a,y_1,h-z_1)} - 2T_{(0,0,0)} = -h\nabla T_z{}^0$ $\boldsymbol{P_3}: T_{(x_1,0,z_1)} + T_{(x_1,0,h-z_1)} - 2T_{(0,0,0)} = -h\nabla T_z{}^0$ $\boldsymbol{P_4}: T_{(x_1,b,z_1)} + T_{(x_1,b,h-z_1)} - 2T_{(0,0,0)} = -h\nabla T_z{}^0$ Periodicity $\Rightarrow \boldsymbol{P_5} - \boldsymbol{P_6}: T_{(x_1,y_1,0)} - T_{(x_1,y_1,h)} = 0$	(8-3)

Table 6 Summary of boundary conditions derived from Path b

	UD			Plain woven			3D4d braided		
	q_x^0	q_y^0	q_z^0	q_x^0	q_y^0	q_z^0	q_x^0	q_y^0	q_z^0
P_1	Uniform	Adiabatic	Adiabatic	Uniform	Adiabatic	Adiabatic	ULC[1]	ULC	ULC
P_2	Uniform	Adiabatic	Adiabatic	Uniform	Adiabatic	Adiabatic	ULC	ULC	ULC
P_3	Adiabatic	Uniform	Adiabatic	Adiabatic	Uniform	Adiabatic	ULC	ULC	ULC
P_4	Adiabatic	Uniform	Adiabatic	Adiabatic	Uniform	Adiabatic	ULC	ULC	ULC
P_5	Adiabatic	Adiabatic	Uniform	Periodic	Periodic	Periodic	Periodic	Periodic	Periodic
P_6	Adiabatic	Adiabatic	Uniform						

[1]ULC: upper and lower constraint

Figure Captions

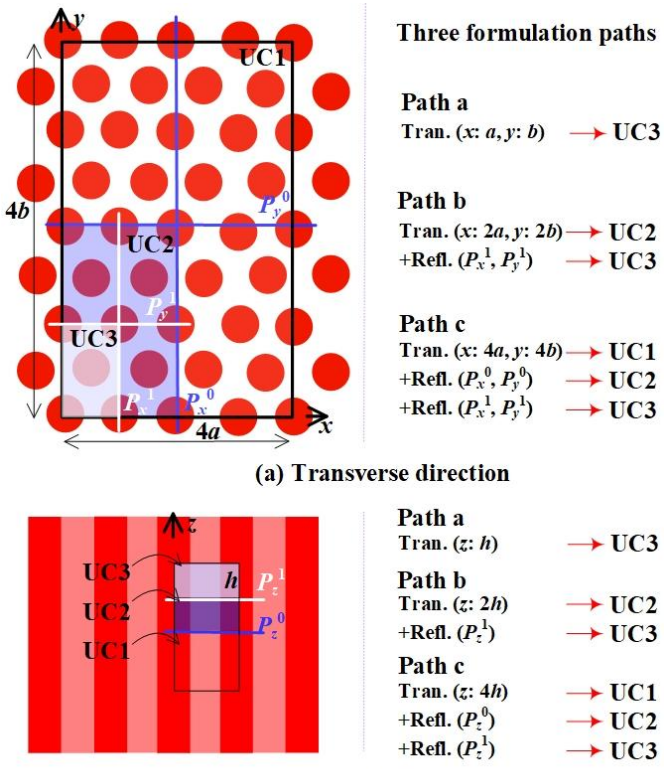

Fig. 1 Paths from UD composite to unit cells

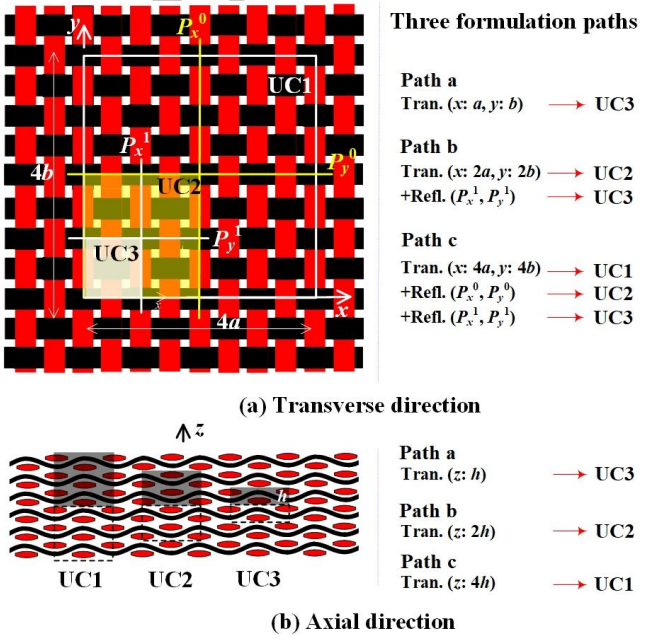

Fig. 2 Paths from plain woven composite to unit cells

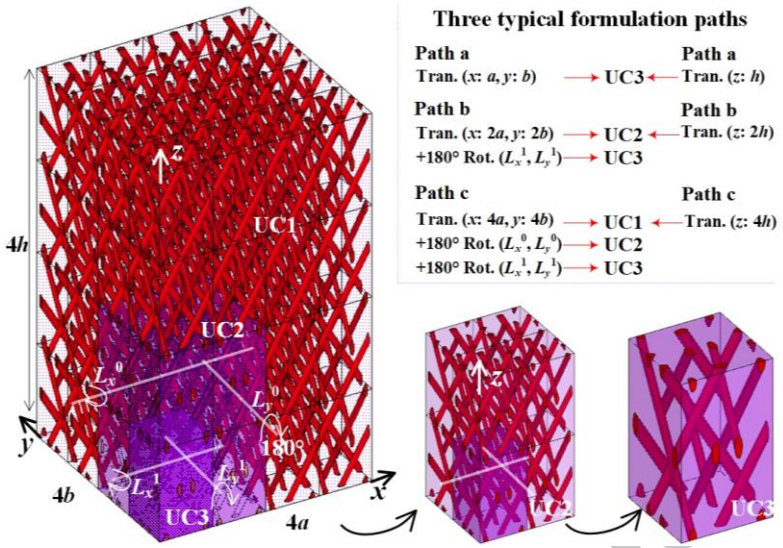

Fig. 3 Paths from 3D four-directional braided composite to unit cells

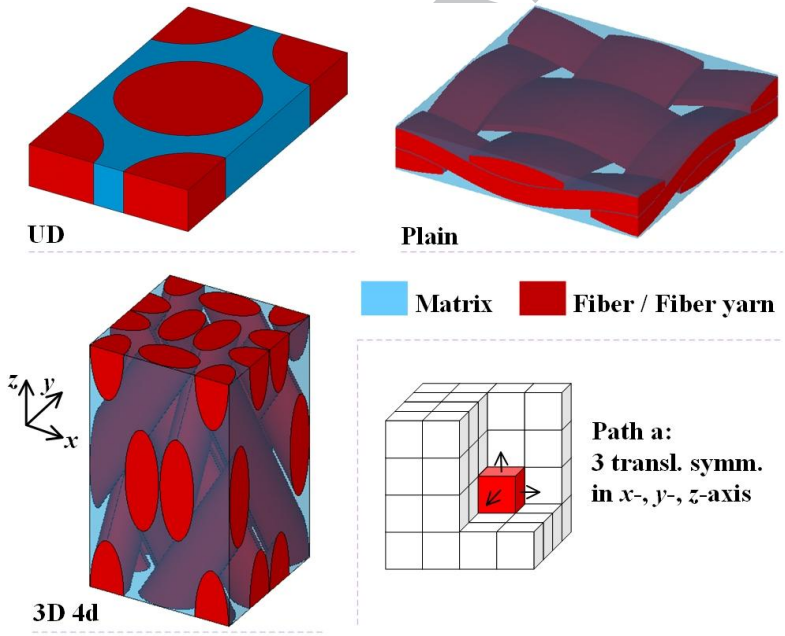

Fig. 4 Unit cell models for three types of composites

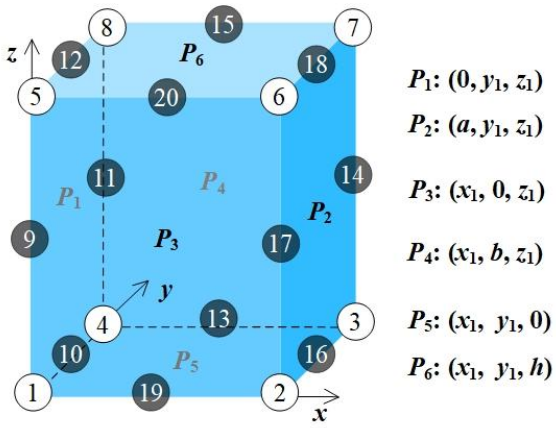

Fig. 5 Boundaries of the unit cell

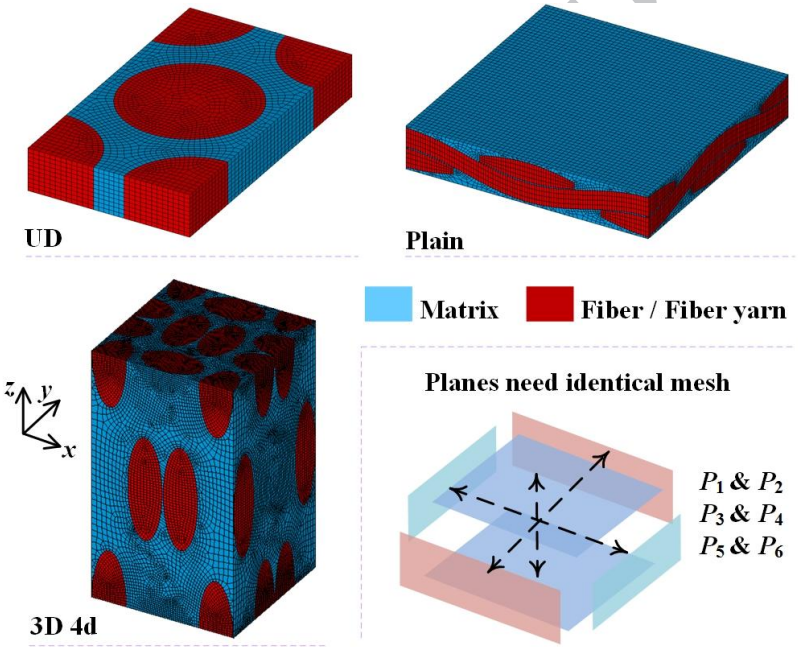

Fig. 6 Meshed models

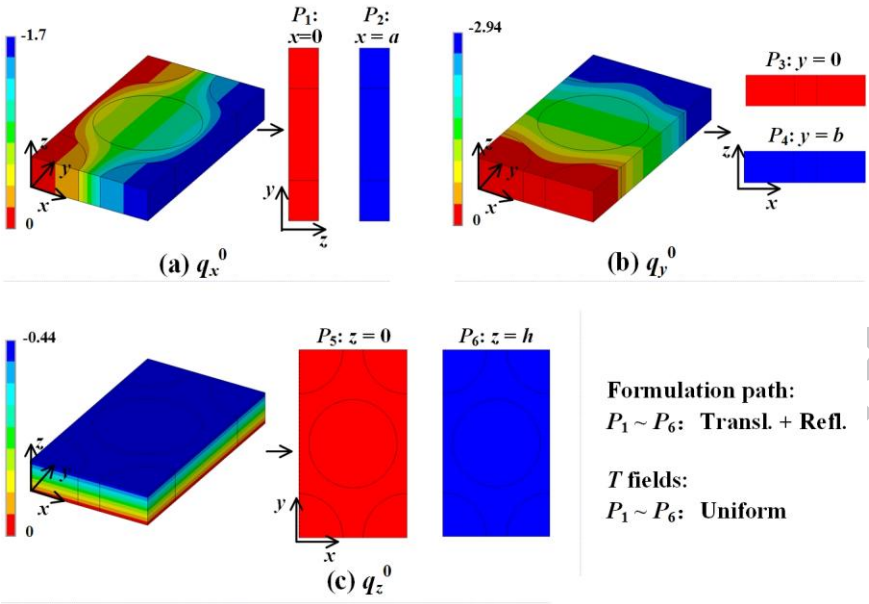

Fig. 7 Temperature fields of UD composites

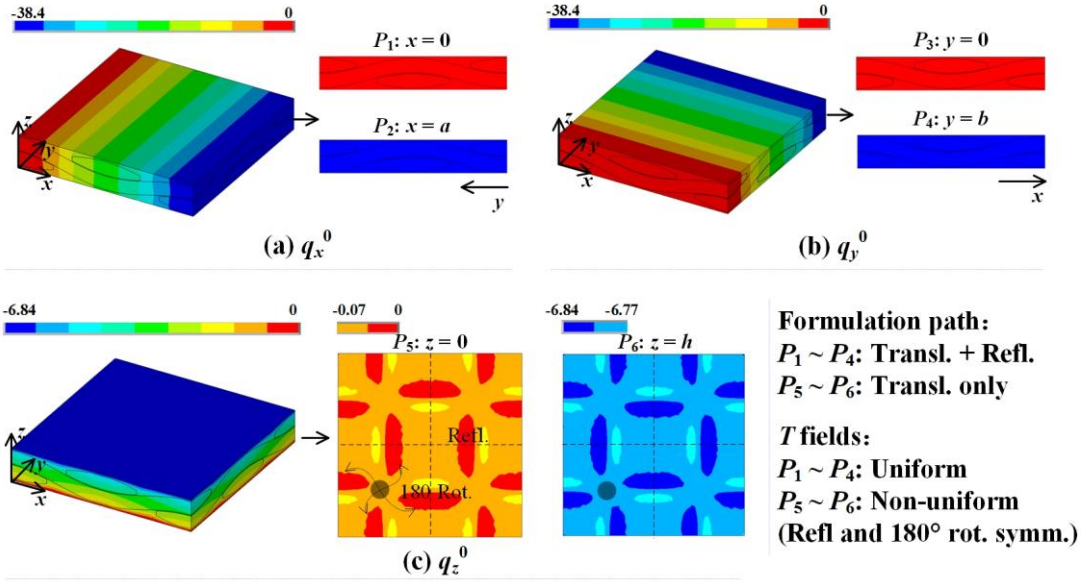

Fig. 8 Temperature fields of plain woven composites

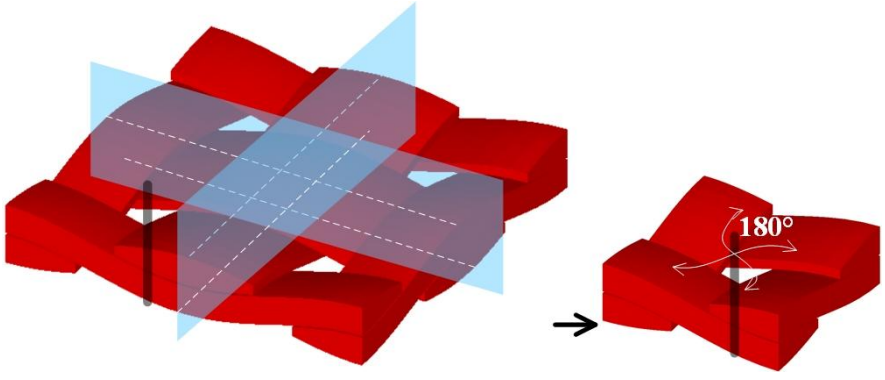

Fig. 9 Further structure symmetries in plain woven composites

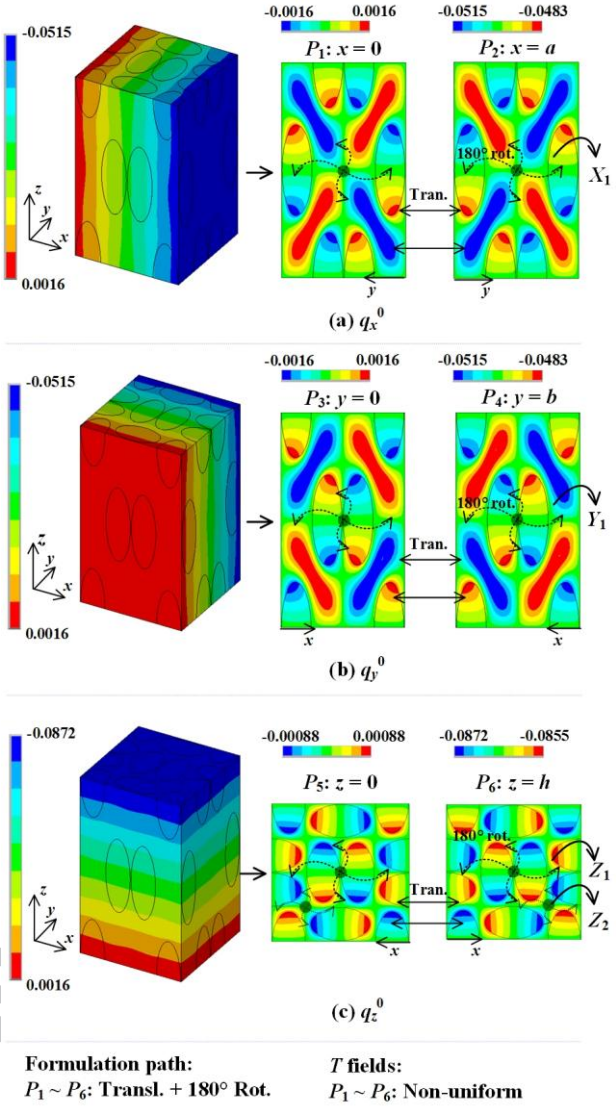

Fig. 10 Temperature fields of 3D four-directional braided composites

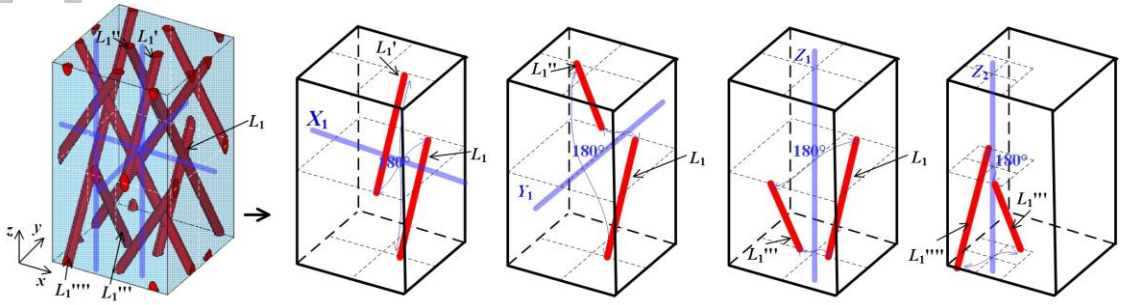

Fig. 11 Further structure symmetries in 3D four-directional braided composites

Highlights

1. The thermal conduction properties of three typical composites are studied based on the unit cell method.
2. The influence of paths on the formulation of unit cells is clarified.
3. The application scope of uniform temperature boundary condition is clarified.